Aerosol choices influence precipitation changes across future scenarios

Isabel L. McCoy[1,1], Mika Vogt[2,2], and Robert Wood[2,2]

[1]University of Miami
[2]University of Washington

November 30, 2022

Abstract

Future precipitation changes are controlled by the atmospheric energy budget, with radiative changes driven by temperature, water vapor, and absorbing aerosol playing dominant roles. Atmospheric energy budgets are calculated for different Shared Socioeconomic Pathways (SSPs) using ScenarioMIP projections from phase 6 of the Climate Model Intercomparison Project and are used to quantify the influence of 21st century aerosol cleanup on precipitation. Absorbing aerosol influences on shortwave absorption are isolated from the effects of water vapor. Apparent hydrologic sensitivity is ˜40% higher for the *Middle of the Road* (SSP2-4.5) scenario with aerosol cleanup than for the *Regional Rivalry* (SSP3-7.0) scenario that maintains aerosol. Regionally, cleanup-induced changes in the atmospheric energy budget are of a similar magnitude to the precipitation increases themselves and are larger than the influence of changes in atmospheric circulation. Policy choices about future absorbing aerosol emissions will therefore have major impacts on global and regional precipitation changes.

Absorbing aerosol choices influence precipitation changes across future scenarios

Isabel L. McCoy[1,2], Mika Vogt[3], and Robert Wood[3]

[1]Rosenstiel School of Marine and Atmospheric Science, University of Miami, Miami, FL, 33149-1031, USA
[2]Cooperative Programs for the Advancement of Earth System Science, University Corporation for Atmospheric Research, Boulder, CO, 80307-3000, USA
[3]Department of Atmospheric Sciences, University of Washington, Seattle, WA, 98195-1640, USA

Key Points:

- Atmospheric energy budgets are used to constrain absorbing aerosol influences on 21st century precipitation in ScenarioMIP projections.
- Shared socioeconomic pathways with aerosol cleanup policies can significantly augment 21st century global precipitation.
- Impacts of regional aerosol changes on precipitation are equal or larger than the influence from atmospheric circulation changes.

Corresponding author: Isabel L. McCoy, imccoy@ucar.edu

Abstract

Future precipitation changes are controlled by the atmospheric energy budget, with temperature, water vapor, and absorbing aerosols playing dominant roles in driving radiative changes. Atmospheric energy budgets are calculated for different Shared Socioeconomic Pathways (SSPs) using ScenarioMIP projections from phase 6 of the Climate Model Intercomparison Project and are used to quantify the influence of 21st century aerosol cleanup on precipitation. Absorbing aerosol influences on shortwave absorption are isolated from the effects of water vapor. Apparent hydrologic sensitivity is ∼40% higher for the *Middle of the Road* (SSP2-4.5) scenario with aerosol cleanup than for the *Regional Rivalry* (SSP3-7.0) scenario that maintains aerosol. Regionally, cleanup-induced changes in the atmospheric energy budget are of a similar magnitude to the precipitation increases themselves and are larger than the influence of changes in atmospheric circulation. Policy choices about future absorbing aerosol emissions will therefore have major impacts on global and regional precipitation changes.

Plain Language Summary

Precipitation changes will have a temperature-dependent and a temperature-independent part of their response to climate change. Water vapor contributes primarily to the former while well-mixed greenhouse gases will influence both. The temperature-independent response will be impacted by absorbing aerosol emissions. This is examined through an atmospheric energy budget where precipitation (i.e., latent heat) balances other energy sources and sinks in the atmosphere (i.e., sensible heat, shortwave and longwave radiation). We utilize a novel set of global climate model simulations that incorporate varied socioeconomic choices over the 21st century to study real-world implications of future aerosol policies on precipitation. Reductions in absorbing aerosol amount help precipitation to increase because less shortwave absorption will occur in the atmosphere and, on average, other energy contributions do not change per degree warming. Global precipitation change per degree of global warming is ∼40% higher for socioeconomic pathways where aerosol cleanup occurs. Regional precipitation changes associated with regional aerosol changes are larger than those associated with changes in atmospheric circulation. Policy choices for aerosol emissions will thus have a critical impact on the future availability of water, both globally and regionally.

1 Introduction

Regional and global changes in precipitation are expected over the 21st century driven by increasing greenhouse gases, changes in aerosols, and changes in land use (Allan et al., 2020). These factors influence precipitation by changing atmospheric longwave emission, shortwave absorption, and surface sensible heat fluxes (Pendergrass & Hartmann, 2014; Allan et al., 2020). A major fraction of the inter-model variance in global mean precipitation increase has been shown to be associated with uncertainties in clear sky shortwave absorption (Pendergrass & Hartmann, 2012; DeAngelis et al., 2015), changes in which are controlled primarily by water vapor path (WVP) and absorbing aerosols.

Emissions of aerosols over the 21st century are expected to change markedly, with changes strongly dependent upon socioeconomic pathways (Lund et al., 2019). WVP increases with global mean temperature, closely following Clausius-Clapeyron (C-C) scaling of ∼7% K^{-1} (Held & Soden, 2006; Allan et al., 2014). Precipitation increases much more slowly with temperature (Held & Soden, 2006) and is constrained by the atmospheric energy budget (Pendergrass & Hartmann, 2014).

Precipitation changes can be separated into temperature-dependent and temperature-independent responses (M. R. Allen & Ingram, 2002; Andrews et al., 2010). WVP contributes primarily to the former as it is strongly tied to temperature. Some aerosols (e.g.,

sulfate) contribute to the temperature-dependent response through scattering sunlight back to space, cooling the surface (Allan et al., 2020). Absorbing aerosols (e.g., black carbon) influence precipitation mostly through the temperature-independent response (Richardson et al., 2018; Allan et al., 2020). Although well-mixed greenhouse gases (WMGHGs) mainly drive the temperature-dependent response, they also contribute to the fast, temperature-independent precipitation response (Richardson et al., 2018).

Climate drivers that significantly influence precipitation through the fast response (e.g., WMGHGs, absorbing aerosols) do so by affecting the atmospheric energy budget. In particular, absorbing aerosols change the amount of shortwave radiation absorbed by the atmosphere and that can impact the surface sensible heat flux. There are other mechanisms by which aerosols are thought to impact precipitation as well. An increase in aerosol amount can lead to a shift from lighter to heavier rain rates and, in the case of absorbing aerosols, a suppression of small clouds and promotion of deeper clouds through increasing instability and convective inhibition. Aerosols are also known to impact circulation patterns, which will influence regional precipitation (Allan et al., 2020). In order to reduce uncertainties in projected precipitation, it is important to understand the role that aerosols play in the poorly-constrained temperature-independent response (Allan et al., 2020). In this study, we focus on understanding how different aerosol policy choices effect precipitation through the fast response.

In the most recent Coupled Model Intercomparison Project (CMIP6), models ran scenarios designated by Shared Socioeconomic Pathways (SSPs) — representing possible policies over the next century — and 2100 forcing levels in W m^{-2} (Eyring et al., 2016). Different policies strongly influence absorbing aerosol changes, impacting future precipitation through the temperature-independent response. These ScenarioMIP simulations (described in Section 2) allow an examination of how policy decisions can influence different aspects of future climate.

We use an atmospheric energy budget framework to estimate contributions from projected changes in absorbing aerosols to changes in global and regional precipitation. We focus especially on two scenarios, SSP2-4.5 and SSP3-7.0, as they offer a contrasting aerosol strategy (cleanup vs. no cleanup, respectively) at intermediate radiative forcing pathways. Section 2 describes the models and methods. Global and regional precipitation change results are presented in Sections 3 and 4, respectively. Section 5 presents a comparison of different methods to constrain the contribution of changes in absorbing aerosols to the precipitation response across scenarios.

2 Materials and Methods

2.1 CMIP6 ScenarioMIP Simulations

We examine climate model projections from four Tier-1 ScenarioMIP scenarios from CMIP6. Each scenario has a distinct SSP and a different level of forcing following the Representative Concentration Pathways (RCPs) used in previous CMIPs (Neill et al., 2016; Riahi et al., 2017). The SSPs factor in differences in societal development related to societal concerns around climate change. Lower SSPs (e.g., SSP1: *Sustainability*, SSP2: *Middle of the Road*) have fewer challenges to climate mitigation and adaptation while higher SSPs have more (e.g., SSP3: *Regional Rivalry*, SSP5: *Fossil-fueled Development*) (Riahi et al., 2017).

SSP1-2.6 uses the RCP2.6 pathway, is the most weakly-forced scenario considered (experiencing less than 2°C warming by 2100 in the multi-model mean), and undergoes substantial land-use change. SSP2-4.5 undergoes intermediate forcing, is an update to RCP4.5, and has less extreme changes in aerosol and land use compared to other SSPs. SSP3-7.0 has a higher forcing (an update to RCP7.0). In particular, it has large land use changes and maintains high emissions of short lived climate forcers (e.g., aerosols) un-

til 2100. Finally, SSP5-8.5 is the most strongly-forced scenario considered, an update to RCP8.5.

Our analysis focuses on changes between the present day (2015-2025) and the end of this century (2090-2100) using composites from 18 CMIP6 models (Table S1). Results are largely insensitive to the length of the averaging period over the range 10-20 years. We have chosen to utilize the 10-year averaging periods in order to leverage the longest record possible from the CMIP6 simulations and thus examine the largest change from the present climate. All currently available models with outputs necessary for estimating absorbing aerosol contributions to the atmospheric energy budget are included, with absorbing aerosol optical depth at 550nm wavelength ($AAOD$) used to describe absorbing aerosol amount. Global changes in key quantities for the four scenarios are listed in Table S2 while trends in CO_2 and WVP and their correspondence are shown in Fig. S1.

The 21st century trend in $AAOD$, which is primarily driven by changes in black carbon emissions, varies strongly across the four scenarios (Fig. 1a). Strong $AAOD$ reductions in SSP1-2.6, SSP2-4.5 reflect aggressive aerosol cleanup policies, weaker reductions occur in SSP5-8.5, and SSP3-7.0 is distinguished by having no $AAOD$ reductions over this period (Turnock et al., 2020). There is larger inter-model variability for $AAOD$ than for the other CMIP6 variables we examine. Some of this is associated with uncertainty in the present-day aerosol state. SSP multi-model mean trends in the anomaly of $AAOD$ from the 2015-2025 period are distinct (Fig. S2a). SSP1-2.6, SSP2-4.5, and SSP5-8.5 models agree on the sign of the global mean $\Delta AAOD$ at 90% confidence ($\sim$16/18 models, Fig. S2b). All CMIP6 models produce a small, near-zero global mean $\Delta AAOD$ for SSP3-7.0 and all model behaviors are distinctly separated from the contrasting SSP2-4.5 case.

All mean and standard error (SE) values from the budget and other calculations are listed in the supplemental tables, S2-S5. Where relevant, mean $\pm$ 2SE values are reported in the text to facilitate comparisons at 95% confidence.

2.2 Absorbing aerosol impacts on the atmospheric energy budget

To quantify the impact of absorbing aerosol changes on precipitation, we adopt an atmospheric energy budget approach (e.g., Pendergrass and Hartmann (2014)). Globally, precipitation change (ΔP) reflects change in atmospheric latent heating (ΔLH), which, together with atmospheric sensible heating (ΔSH), must be balanced by reductions in absorbed energy in the net atmospheric longwave (ΔLW) and shortwave (ΔSW):

$$-L_v \Delta P = -\Delta LH = \Delta SH + \Delta SW + \Delta LW \tag{1}$$

where L_v is the latent heat of vaporization. Water vapor and absorbing aerosol changes dominate ΔSW (Richardson et al., 2018). We use a multiple regression to separate these contributions. For each scenario, global annual multi-model mean time series of WVP, $AAOD$ and net SW are constructed. The resulting fit, parabolic in ΔWVP and linear in $\Delta AAOD$, explains 99.8% of the variance of ΔSW at 95% confidence (Fig. S3):

$$\Delta SW = a \cdot \Delta WVP + b \cdot (\Delta WVP)^2 + c \cdot \Delta AAOD \tag{2}$$

where a = 0.693 $\pm$ 0.009 W kg^{-1}, b = -0.016 $\pm$ 0.001 W kg^{-2} m^2, and c = 520 $\pm$ 9 W m^{-2}, with errors providing 95% confidence intervals. We note that c, which is computed for all models together, is within the standard error of the multi-model mean atmospheric absorption dependence on $AAOD$ found in CMIP5 AeroCom models, 525 $\pm$ 92 W m^{-2} (see Table 3 in Myhre et al., 2013). The quadratic term in ΔWVP is needed to account for the sub-linear dependency of solar absorption on WVP (Lacis & Hansen, 1974) but is relatively weak, contributing only 5-15% of the overall ΔWVP contribution to SW absorption.

3 Changes in Global Precipitation over the 21st century

Within each scenario (i.e., for fixed radiative forcing), global mean precipitation ΔP increases at ∼2.5% per degree of global mean warming (Fig. 1b) consistent with 2-3% K^{-1} in earlier studies (Samset et al., 2018). Although this slope (i.e., the hydrologic sensitivity, η), is consistent across SSPs (Table S2), the intercepts of the ensemble member fits differ significantly. The SSP differences in response can also be described by the apparent hydrologic sensitivity, $\eta_a = L_v \Delta P / \Delta T$ (Allan et al., 2020), using the multi-model means (Table S2). SSP3-7.0 stands out as it has a substantially lower ΔP than would be expected from the ΔT experienced in this scenario (1.30 ± 0.14 W m^{-2} K^{-1}). Indeed, instead of falling between SSP2-4.5 (1.76 ± 0.14) and SSP5-8.5 (1.39 ± 0.14), the SSP3-7.0 line nearly overlaps the SSP5-8.5 line (Fig. 1b).

To explore this further, Fig. 1c shows multi-model mean changes in the atmospheric budget terms for the four scenarios (Table S2). As ΔT increases, all terms correspondingly increase in magnitude. Negative ΔLW indicates increasing atmospheric radiative cooling as temperature increases (Pendergrass & Hartmann, 2014), which is remarkably linear in ΔT. In contrast, changes in ΔSW, ΔSH, and ΔLH ($\equiv L_v \Delta P$) all show deviations from linear behavior. Specifically, SSP3-7.0 has a markedly stronger increase in ΔSW (3.51 ± 0.34 W m^{-2}) and, as a result, a muted increase in ΔLH (3.86 ± 0.38 W m^{-2}) and thus precipitation at this ΔT (3.00 ± 0.30 K). The lack of deviation by ΔLW (-6.24 ± 0.62 W m^{-2}) in SSP3-7.0 suggests that anomalies in WMGHGs and WVP are unlikely to be driving the anomalous precipitation response in SSP3-7.0. Instead, ΔSW is likely a major driver of the unusual behavior seen in SSP3-7.0 ΔP (Fig. 1b, c). The lack of aerosol cleanup in this scenario (Fig. 1a) may be muting precipitation increases over the 21st century compared with scenarios that undergo cleanup.

We examine two scenarios in detail, SSP2-4.5 and SSP3-7.0, that represent intermediate RCP pathways in the ScenarioMIP simulations but with substantially different SSP aerosol emission choices. Using Eq. 2, we quantify the contributions of $\Delta AAOD$ (ΔSW_{AAOD}) and ΔWVP (ΔSW_{WVP}) to ΔSW. These are shown along with the remaining energy budget terms from Eq. 1 in Fig. 2. To control for differences in forcing (i.e., temperature change) between scenarios, energy budgets are examined per degree of global warming and terms are reported as sensitivities (Table S3). The normalized precipitation change (i.e., apparent hydrologic sensitivity) is ∼40% larger for SSP2-4.5 (1.8 ± 0.6 W m^{-2} K^{-1}) than for SSP3-7.0 (1.3 ± 0.4 W m^{-2} K^{-1}). ΔLW (-2.2 vs. -2.1 ± 0.6 W m^{-2} K^{-1}) and ΔSW_{WVP} (1.1 ± 0.4 W m^{-2} K^{-1}) sensitivities are remarkably similar between these scenarios, indicating they are not the primary drivers of differences in η_a. Instead, the difference in η_a can be explained by differences in absorbing aerosol pathways between the two scenarios, SSP2-4.5 (Fig. 2a) and SSP3-7.0 (Fig. 2b): ΔSW_{AAOD} is the major contributor to the difference (-0.50 ± 0.14 vs. 0.026 ± 0.014 W m^{-2} K^{-1}) but ΔSH also has a small contribution (-0.19 ± 0.06 vs. -0.33 ± 0.1 W m^{-2} K^{-1}). Aerosol cleanup in SSP2-4.5 reduces SW absorption (0.64 ± 0.18 vs 1.2 ± 0.4 W m^{-2} K^{-1} for SSP3-7.0), offsetting approximately 60% of the increased SW absorption driven by increased WVP and increasing the amount of SW that can contribute to the surface SH. This results in a larger global precipitation increase in SSP2-4.5 while the lack of cleanup in SSP3-7.0 results in a muted 21st century precipitation increase.

4 Factors Influencing Regional Precipitation Changes

Given that aerosol cleanup choices can significantly effect global precipitation changes, we now explore the extent to which regional $\Delta AAOD$ is expected to influence regional precipitation over the 21st century. Geographic patterns of $\Delta AAOD$ are highly heterogeneous. We focus on two regions with striking 21st century $\Delta AAOD$ (Table S4, Fig. S4), which are also thought to be dominated by the temperature-independent precipitation response (Samset et al., 2016): Southeastern Asia (0-45°N, 60-130°E) and Equatorial

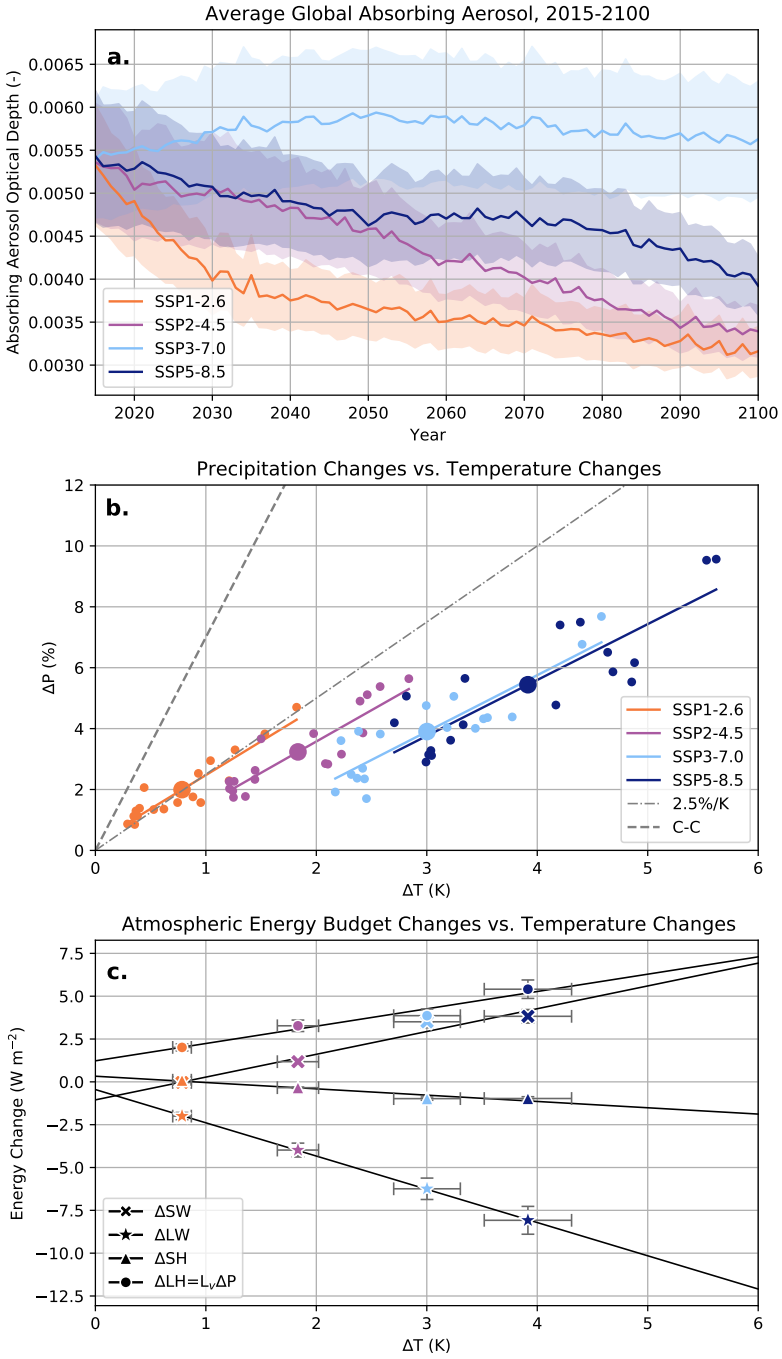

Figure 1. (a) Global multi-model ensemble mean (line) and corresponding standard error (shading) for *AAOD* by scenario across period of interest (2015-2100). Global mean changes in (b) precipitation and (c) atmospheric energy budget terms plotted as a function of global mean surface air temperature changes (Table S2). Changes are computed as the difference between two ten-year periods, 2090-2100 and 2015-2025. In (b), projections from each contributing model (small circles) and the scenario multi-model mean (large circles) are shown. The ratio of the ensemble mean $\Delta P/\Delta T$ represents the apparent hydrologic sensitivity. The slope of the best fit line through the individual ensemble members for each scenario represents the hydrologic sensitivity (Table S2), which is ∼2.5% K^{-1} for each scenario (dot-dash). The C-C response (i.e., ∼7% K^{-1}) is included for reference (dash). In (c), one SE is used to indicate uncertainty in the multi-model mean budget terms while maintaining visual clarity.

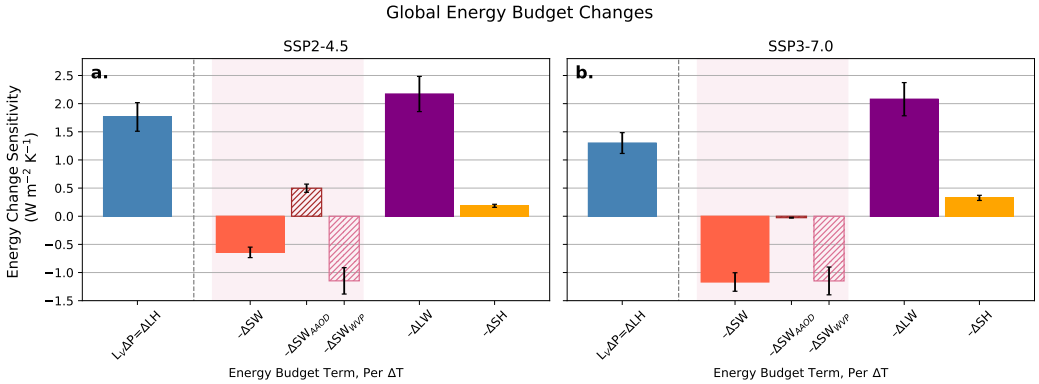

Figure 2. Global changes in the atmospheric energy budget (2015-2025 to 2090-2100) for two scenarios with contrasting aerosol choices: (a) SSP2-4.5 and (b) SSP3-7.0 (Table S3). Energy budget terms are normalized by the change in global mean surface air temperature and expressed as sensitivities. ΔSW (solid) is decomposed into two (hatched) components, ΔSW_{AAOD} and ΔSW_{WVP}, based on Eq. 2. Solid bars on the right of the dashed line sum to the precipitation change on the left following Eq. 1. Bars represent multi-model means while error bars represent 2SE based on the variability in the multi-model mean 10-year periods propagated through the change and normalization calculations. Standard errors for ΔSW components also include coefficient uncertainties.

Africa (15°S-15°N, 30°W-30°E). Strong aerosol cleanup occurs in both regions in SSP2-4.5 (-9.12 ± 0.98 and -4.98 ± 0.58 $\cdot 10^{-3}$, respectively) with ∼90% of models agreeing in the sign of the multi-model mean regional $\Delta AAOD$ (Fig. S5b, S6b). In SSP3-7.0, aerosol loadings increase in Equatorial Africa (2.97 ± 0.3 $\cdot 10^{-3}$) and decrease slightly in SE Asia (-1.74 ± 0.36 $\cdot 10^{-3}$). Although the $\Delta AAOD$ is smaller in this scenario, most models still agree in sign of the mean change over the region (Fig. S5c, S6c). The consistency across CMIP6 models in regional behavior for these SSPs supports our choice in selecting these areas to study.

The regions studied here are sufficiently large (>3000 km in scale) that atmospheric energy and water budgets are useful for assessment of their precipitation changes (Dagan et al., 2019a; Dagan & Stier, 2020). On a regional scale the energy and moisture budgets are:

$$L_v \Delta P = -\Delta SH - \Delta SW - \Delta LW + \Delta div(s) \quad (3)$$

$$\Delta P = \Delta E - \Delta div(q_v) = \Delta LH / L_v - \Delta div(q_v) \quad (4)$$

where $div(s)$ and $div(q_v)$ are residuals representing the divergences of dry static energy and column integrated moisture, respectively, reflecting the exports of energy and moisture required to balance the regional budgets.

Fig. 3 and Table S5 present contributions of each of the normalized terms in Eqns. 3 and 4 to the overall, normalized ΔP experienced in each region under SSP2-4.5(4.0 ± 1.2 vs. 1.6 ± 0.6 W m^{-2} K^{-1} in SE Asia vs. Equatorial Africa) and SSP3-7.0 (2.6 ± 0.8 vs. 1.3 ± 0.6). Examining the simpler water budget (Eq. 4) first, we find ΔLH sensitivity differs between SSPs but not regionally: SSP2-4.5 (2.8 vs. 2.7 ± 0.8 W m^{-2} K^{-1} in SE Asia vs. Equatorial Africa) has a larger change than SSP3-7.0 (1.7 vs. 1.6 ± 0.4). However, $\Delta div(q_v)$ sensitivity varies more between regions than by SSP: SE Asia experiences increased moisture convergence (-1.1 ± 1.2 vs. -0.9 ± 0.8 W m^{-2} K^{-1} in SSP2-4.5 vs. SSP3-7.0) while Equatorial Africa experiences the opposite (1.2 ± 0.8 vs. 0.3 ± 0.6). The net result is a substantial variation between both region and scenario for regional η_a.

Figure 3. Regional atmospheric energy and moisture budget changes (2015-2025 to 2090-2100) for SSP2-4.5 (panels a, c) and SSP3-7.0 (panels b, d) for Southeast Asia (0-45°N, 60-130°E; panels a, b) and Equatorial Africa (15°S-15°N, 30°W-30°E; panels c, d) (Table S5). Budget term normalization, ΔSW decomposition, bar and error bar meanings as in Fig. 2. Normalized energy budget terms (solid bars between dashed lines) sum to the normalized precipitation change (left) following Eq. 3 while normalized water budget terms (solid bars to the right of dashed lines) sum following Eq. 4.

The regional energy budget provides insight into variability in regional η_a (Fig. 3). As in the global budget (Fig. 2), ΔLW (SE Asia: -2.4 ± 0.6 vs. -2.6 ± 0.8 W m^{-2} 4 K^{-1} in SSP2-4.5 vs. SSP3-7.0; Equatorial Africa: -2.7 vs. -2.5 ± 0.8) and ΔSW_{WVP} (SE Asia: 1.5 ± 0.8 for both; Equatorial Africa: 1.7 vs. 1.6 ± 1.0) variation across region and SSP is very small compared to other, more explicit differences between terms. WMGHGs and WVP may have more complex influences on the regional and inter-scenario differences in precipitation response, for example by affecting regional circulation patterns as discussed below. Instead, ΔSW_{AAOD}, ΔSH, and $\Delta div(s)$ differences appear to drive the majority of the variability in regional η_a.

Absorbing aerosol driven changes in SW absorption (ΔSW_{AAOD}) are the leading contributor to energy budget changes between the two scenarios in both regions as can be seen by comparing left versus right panels in Fig. 3 (SE Asia: -2.6 ± 0.8 vs. -0.30 ± 0.14 W m^{-2} K^{-1} in SSP2-4.5 vs. SSP3-7.0; Equatorial Africa: -1.4 ± 0.4 vs. 0.51 ± 0.14). The smaller contributions from ΔSH (SE Asia: 0.58 ± 0.18 vs. -0.11 ± 0.04; Equatorial Africa: 0.47 ± 0.16 vs. -0.14 ± 0.06), and $\Delta div(s)$ (SE Asia: 1.5 ± 1.2 vs. 1.0 ± 0.8; Equatorial Africa: -0.6 vs. 0.3 ± 0.8) may also be associated with aerosol changes through influencing SW availability at the surface and regional circulation patterns. Overall, this implies that a substantial fraction of the markedly higher regional η_a for SSP2-4.5 vs. SSP3-7.0 can be explained by aerosol cleanup policies. Note that this applies in both regions even though

aerosol loadings increased in SSP3-7.0 in Equatorial Africa while SE Asia experienced a smaller cleanup in SSP3-7.0 than in SSP2-4.5.

Aerosol forcing can impact circulation, and thus precipitation, changes in Equatorial Africa through shifting the location of the inter-tropical convergence zone (R. J. Allen et al., 2015; Chemke & Dagan, 2018; Wang, 2015) and in SE Asia through changing the monsoon circulation (Bollasina et al., 2011). Increased $AAOD$ in the tropics may influence precipitation through thermally driven circulation changes from modification of $div(s)$ (Dagan et al., 2019b, 2021) but absorbing aerosol perturbations over Equatorial Africa and SE Asia are expected to have a small effect (Dagan et al., 2021). Indeed, changes in both $\Delta div(s)$ and $\Delta div(q_v)$ sensitivity (SE Asia: -1.1 $\pm$ 1.2 vs. -0.9 $\pm$ 0.8 W m^{-2} K^{-1} in SSP2-4.5 vs. SSP3-7.0; Equatorial Africa: 1.2 $\pm$ 0.8 vs. 0.3 $\pm$ 0.6) between scenarios are considerably smaller than those in ΔSW_{AAOD}. This implies that regional precipitation changes between scenarios are more strongly controlled by aerosol absorption changes than they are by changes in the import or export of energy and moisture, suggestive of a relatively small role for atmospheric circulation changes.

To better understand the circulation responses, we estimate the thermodynamic contribution to precipitation-evaporation ($P-E$) changes that would occur in the absence of changes in the lower tropospheric circulation. Using Eq. 5, we estimate the moisture convergence $\Delta div(q_v)_{thermo}$ driven solely by increased WVP (Fig. 4) assuming the circulation remains fixed (i.e., Held and Soden (2006)):

$$\Delta(P-E) \approx \alpha(P-E)\Delta T = -\Delta div(q_v)_{thermo} \tag{5}$$

where E is evaporation and $\alpha \approx 0.07$. We use $\Delta div(q_v)_{thermo}$ in Eq. 4 to estimate a predicted change in precipitation, ΔP_{thermo}, absent circulation changes. The difference, $\Delta P_{circ} = \Delta P - \Delta P_{thermo}$, is an estimate of the influence that circulation has on regional precipitation. Similarly, the difference $\Delta div(q_v)_{circ} = \Delta div(q_v) - \Delta div(q_v)_{thermo}$ is an estimate of the circulation influence on regional moisture convergence changes.

Comparing the magnitude of the circulation change influence on precipitation (ΔP_{circ}, SE Asia: -0.8 $\pm$ 1.6 vs. -1.0 $\pm$ 1.0 W m^{-2} K^{-1} in SSP2-4.5 vs. SSP3-7.0; Equatorial Africa: -0.6 $\pm$ 1.2 vs. 0.3 $\pm$ 0.8) to the magnitude of the AAOD influence on SW (ΔSW_{AAOD}), we conclude that the influence of aerosol cleanup (SSP2-4.5) has a larger influence on ΔP than do changes in circulation for both Equatorial Africa and SE Asia (Fig. 4 a, c, Tables S4, S5). When aerosol emissions follow a regional rivalry framework (SSP3-7.0), the influence of aerosol radiative changes is of an equivalent magnitude to circulation changes in Equatorial Africa (where aerosol increases) and is smaller than the circulation influence in SE Asia (where aerosol still reduces but by a smaller magnitude than in SSP2-4.5) (Fig. 4 b, d, Tables S4, S5). Although circulation changes clearly influence regional precipitation trends over the 21st century on spatial scales of several thousand kilometers, such changes are unlikely to exceed those driven by local cleanup efforts in regions with high loadings of absorbing aerosol.

Our estimate of the influence of aerosol cleanup on regional precipitation is likely a lower bound. This is because we only explicitly account for the effect of aerosol changes on precipitation through SW absorption and have not separately estimated the circulation change resulting from the remote and local coupling to aerosol forcing that is expected to influence these regions. However, our results do indicate that we should expect that, through SW absorption, SH flux, and circulation changes, aerosol cleanup (in SSP2-4.5, compared with SSP3-7.0) will accelerate increases in precipitation in both regions examined.

5 Quantifying absorbing aerosol influences on precipitation

These atmospheric energy budget examinations provide compelling evidence that future choices in aerosol emissions will influence precipitation over the 21st century, both

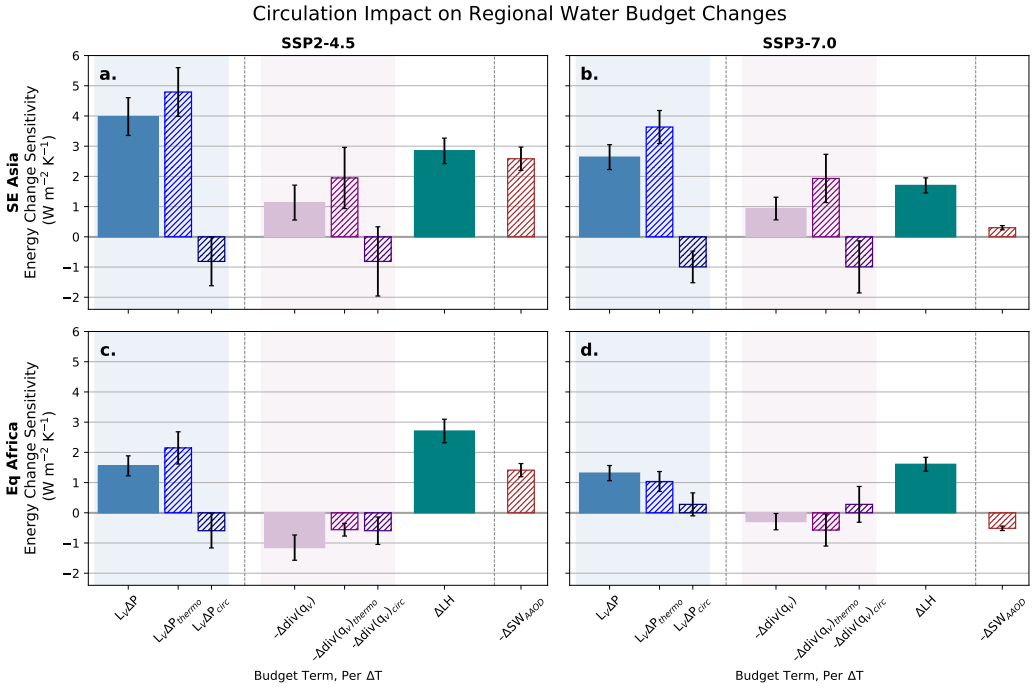

Figure 4. Estimation of regional changes in circulation (2015-2025 to 2090-2100) for SSP2-4.5 (a, c) and SSP3-7.0 (b, d) for Southeast Asia (a, b) and Equatorial Africa (c, d) (Table S5). Budget term normalization, bar and error bar meanings as in Fig. 3. Thermodynamic ($\Delta div(q_v)_{thermo}$, ΔP_{thermo}) and circulation ($\Delta div(q_v)_{circ}$, ΔP_{circ}) contributions to the total ($\Delta div(q_v)$, ΔP) are estimated using Eqns. 5 and 4. ΔSW_{AAOD} (Fig. 3), the only ΔSW component changing between regions and SSPs, is included for reference.

regionally and globally. Absorbing aerosol, via ΔSW, affects precipitation mostly through the fast (i.e., temperature-independent) response (M. R. Allen & Ingram, 2002). In this section, we quantify the fast response associated with $\Delta AAOD$ using three different analysis methods (Fig. 5, Table S2).

The first and simplest method uses multiple linear regression to establish temperature-dependent and AAOD-dependent influences on ΔP (Fig. 5a). This regression explains 86% of the variance in global ΔP across all SSPs at 95% confidence. Using the coefficient for the $\Delta AAOD$ contribution, we estimate the aerosol-driven portion of ΔP (ΔP_{AAOD}) for each scenario (Fig. 5b).

The second method follows Allan et al. (2020), producing an independent estimate of the fast response that does not use $\Delta AAOD$. We estimate the temperature-dependent precipitation response (η) and the combined temperature-dependent and independent response (η_a) from Fig. 1b (see Section 3). The fast precipitation response for SSPs is the difference between these hydrologic sensitivities:

$$\Delta P_{fast} = \Delta T \left(\eta - \eta_a\right). \tag{6}$$

Table S2 shows η, η_a, and ΔP_{fast} global estimates by scenario. We expect η to be scenario independent since it is a model-specific quantity and all SSP simulations use the same set of CMIP6 models. Indeed, individual SSP η's are within uncertainties of each other. For consistency in our calculations, we use the scenario mean value for all

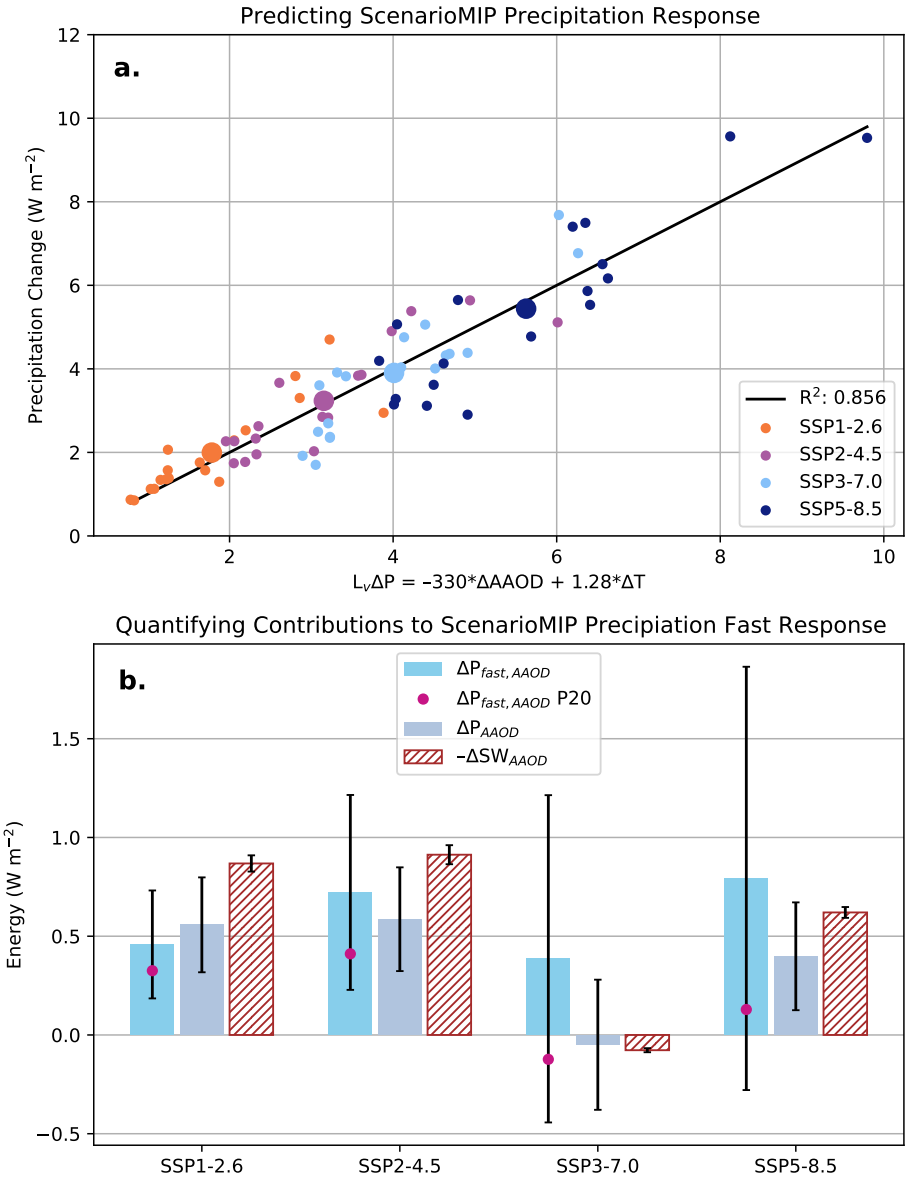

Figure 5. Quantifying the fast precipitation responses in ScenarioMIP simulations through various methods (Table S2). (a) A multiple linear regression on $\Delta AAOD$ and ΔT for global ensemble members across all SSPs explains 86% of the variance at 95% confidence of the total precipitation response, ΔP. (b) Using the relationship in (a), we estimate the AAOD contribution, ΔP_{AAOD}, and contrast it with estimates of $\Delta P_{fast,AAOD}$, explained in the text, and ΔSW_{AAOD}. The $\Delta P_{fast,AAOD}$ P20 comparison (red circle) uses η=2.16 (Pendergrass, 2020) instead of 2.02 W m^{-2} K^{-1} (this study). All of these temperature-independent energy terms are significantly smaller for SSP3-7.0 than in the other SSPs, signifying the importance of $\Delta AAOD$ in determining ΔP. Bars represent multi-model mean and errors represent one SE instead of 2SE to account for large uncertainty in $\Delta P_{fast,AAOD}$ for SSP5-8.5.

SSPs, $\overline{\eta_{SSP}}$=2.02 ± 0.26 W m^{-2} K^{-1} (Table S2). This is within uncertainties of a multi-model mean estimate from abrupt 4xCO2 CMIP6 simulations, η=2.16 W m^{-2} K^{-1} (Pendergrass, 2020).

The fast response includes contributions from changes in absorbing aerosols as well as WMGHGs, most importantly ΔCO_2 and, to a lesser extent, ΔCH_4 and other WMGHG:

$$\Delta P_{fast} = \Delta P_{fast,AAOD} + \Delta P_{fast,CO2} + \Delta P_{fast,CH4} + \Delta P_{fast,other}. \quad (7)$$

To calculate $\Delta P_{fast,AAOD}$ for each scenario from Eq. 7, we use ΔP_{fast} estimates (Table S2) and assume $\Delta P_{fast,other}$ is negligible. We rely on Richardson et al. (2018)'s sensitivity studies to estimate fast precipitation responses for the two dominant WMGHGs (CO_2 and CH_4): a doubling of CO_2 has a -2.2 W m^{-2} response while a tripling of CH_4 has -0.5 W m^{-2} (see their Fig. 1). Assuming contributions of CO_2 and CH_4 to the fast response depend logarithmically on concentration (consistent with Andrews et al. (2010) and Laakso et al. (2020)), we construct the following equations for fast responses from arbitrary gas concentration changes:

$$\Delta P_{fastCO2} = -\left(\frac{2.2}{\ln 2}\right)\ln\left(\frac{[CO_2^f]}{[CO_2^i]}\right)$$
$$\Delta P_{fastCH4} = -\left(\frac{0.5}{\ln 3}\right)\ln\left(\frac{[CH_4^f]}{[CH_4^i]}\right) \quad (8)$$

Superscripts i and f in Eq. 8 indicate initial (2015-2025 mean) and final (2090-2100 mean) concentrations, respectively. $[CO_2]$ and $[CH_4]$ are the respective gas concentrations for CO_2 and CH_4 from Meinshausen et al. (2020). These contributions to ΔP_{fast} and the final $\Delta P_{fast,AAOD}$ (Fig. 5b) are listed in Table S2 by scenario. We also include an estimate of $\Delta P_{fast,AAOD}$ in Fig. 5b using η from Pendergrass (2020) (P20) that falls within uncertainties, suggesting $\Delta P_{fast,AAOD}$ is not overly sensitive to our η determination.

The only other WMGHG that contributes significantly to the atmospheric energy budget is nitrous oxide (N_2O), but estimates of its impact on fast precipitation responses are not available in the literature. The TOA forcing from N_2O over the 21st century is estimated to be less than 0.3 W m^{-2} for all SSPs studied here (Meinshausen et al., 2020). Assuming the fast precipitation response from N_2O scales similarly with TOA forcing as for other WMGHG (CO_2 and CH_4), then $\Delta P_{fast,N2O}$ would range from -0.05 W m^{-2} in SSP1-2.6 to -0.13 W m^{-2} in SSP3-7.0. The small range and magnitude of these estimated responses, and the significant statistical uncertainties in the estimates of ΔP_{fast} (Table S2), justifies our choice to exclude the effects of N_2O from our estimates of $\Delta P_{fast,AAOD}$.

The third method relies on the idea that changes in atmospheric SW absorption from aerosol (ΔSW_{AAOD}) translate into precipitation changes in the absence of changes in the other energy budget terms (ΔSH, ΔLW, and ΔSW_{WVP}). This neglects the influence that an increase in SW absorption associated with an increase in absorbing aerosol will have on the SH flux through reducing the amount of SW that reaches the surface, a much smaller effect (Fig. 2). Since the relative changes in these other terms are small across scenarios (Figs. 1, 2, Table S2), ΔSW_{AAOD} is an approximate estimate of the global ΔP due to absorbing aerosol changes (Fig. 5b).

Despite the large uncertainty in the residual estimation of $\Delta P_{fast,AAOD}$, we find relatively good agreement across scenarios between $\Delta P_{fast,AAOD}$ and ΔP_{AAOD} determined from regressing ΔP against ΔT and $\Delta AAOD$ (Fig. 5b). All methods agree that SSP3-7.0 has a precipitation response to AAOD that is very small compared with other scenarios, consistent with little global aerosol cleanup (Fig. 1a). The variation of precipitation response to $\Delta AAOD$ across scenarios is also consistent with our independent expectations from the atmospheric energy budget, as shown by reductions in shortwave absorption by aerosol (ΔSW_{AAOD} <0) over the 21st century in all scenarios except SSP3-7.0 (Fig. 5b).

The general agreement between the three approaches to estimating absorbing aerosol influences on 21st century precipitation changes from ScenarioMIP simulations provides confidence that aerosol cleanup policies can lead to global precipitation rate increases in excess of 0.5 W m^{-2} (≈0.6% increases on present day rates). Although this is relatively modest when compared with precipitation increases projected for the higher radiative forcings (e.g., ∼6% in SSP5-8.5 by the end of the century), if policies for CO_2 mitigation are more aggressive, then absorbing aerosol cleanup will constitute a much stronger contribution to precipitation increases in the coming century.

6 Summary

We use data from the ScenarioMIP suite of CMIP6 model simulations to explore the influence of absorbing aerosols on precipitation changes for four scenarios over the 21st century. Atmospheric energy and water budgets are used to examine influences of different controls on precipitation, both globally and regionally, between 2015-2025 and 2090-2100. As expected, precipitation increases of 2-3% K^{-1} (Fig. 1) are typical because atmospheric radiative cooling is unable to keep pace with water vapor increases, which follow Clausius-Clapeyron. Precipitation increases are greater for scenarios with strong 21st century aerosol cleanup. We use a regression approach to isolate the temperature-independent effects of absorbing aerosol on the shortwave energy budget from the temperature-dependent effects of water vapor. We show that the apparent global hydrologic sensitivity is 40% stronger in SSP2-4.5 (aerosol cleanup) than in SSP3-7.0 (no cleanup), and this can be explained primarily by reduced 21st century SW absorption by aerosol in the former scenario (Fig. 2).

This absorbing aerosol influence is found to significantly affect precipitation at the regional scale (Fig. 3). Two regions are examined, Equatorial Africa (15°S-15°N, 30°W-30°E) and Southeast Asia (0-45°N, 60-130°E), both of which experience aerosol cleanup during SSP2-4.5 but have differing aerosol emissions in SSP3-7.0. The influence of aerosol cleanup on precipitation via atmospheric shortwave absorption is estimated to be larger than the impacts of circulation changes in both regions (Fig. 4).

The influence of absorbing aerosols on precipitation through the fast, temperature-independent response is quantified for all ScenarioMIP projections using both the hydrologic sensitivity and a multiple linear regression against ΔT and $\Delta AAOD$ (Fig. 5). Estimates are consistent with atmospheric energy budget estimations of $AAOD$ influence, suggesting absorbing aerosol cleanup policies are likely to boost global precipitation responses by at least 0.5 W m^{-2} (≈0.6% of the present-day global mean rate). For scenarios with aggressive greenhouse gas mitigation (lower forcing, i.e., SSP1-2.6 and SSP2-4.5), the aerosol-driven increases in precipitation can significantly contribute to the increases expected from climate warming through the fast-response. This study highlights the importance of considering aerosol emissions in future policy decisions as those choices will have critical and long-lasting impacts on both global and regional precipitation and, as a result, water availability in the future.

Acknowledgments

We thank Angeline Pendergrass and Dargan Frierson for helpful discussions of this work. We also acknowledge the World Climate Research Programme and its Working Group on Coupled Modelling for coordinating CMIP6; the climate modeling groups involved for their simulations; the Earth System Grid Federation (ESGF) for archiving and facilitating data usage; and the multiple funding agencies who support CMIP and ESGF efforts. Research by ILM is supported by the NOAA Climate and Global Change Postdoctoral Fellowship Program, administered by UCAR's Cooperative Programs for the Advancement of Earth System Science (CPAESS) under award NA18NWS4620043B. MV was funded on indirect cost recovery support from grants to UW.

Data Availability: All CMIP6 ScenarioMIP simulations used in this study are available at https://esgf-node.llnl.gov/projects/cmip6/.

References

Allan, R. P., Barlow, M., Byrne, M. P., Cherchi, A., Douville, H., Fowler, H. J., ... Zolina, O. (2020). Advances in understanding large-scale responses of the water cycle to climate change [Journal Article]. *Ann N Y Acad Sci*, *1472*(1), 49-75. Retrieved from https://www.ncbi.nlm.nih.gov/pubmed/32246848 doi: 10.1111/nyas.14337

Allan, R. P., Liu, C., Zahn, M., Lavers, D. A., Koukouvagias, E., & Bodas-Salcedo, A. (2014, May). Physically Consistent Responses of the Global Atmospheric Hydrological Cycle in Models and Observations. *Surveys in Geophysics*, *35*(3), 533–552. Retrieved 2021-08-24, from https://doi.org/10.1007/s10712-012-9213-z doi: 10.1007/s10712-012-9213-z

Allen, M. R., & Ingram, W. J. (2002). Constraints on future changes in climate and the hydrologic cycle [Journal Article]. *Nature*, *419*(6903), 228-232. Retrieved from https://doi.org/10.1038/nature01092https://www.nature.com/articles/nature01092a.pdf doi: 10.1038/nature01092

Allen, R. J., Evan, A. T., & Booth, B. B. B. (2015). Interhemispheric aerosol radiative forcing and tropical precipitation shifts during the late twentieth century [Journal Article]. *Journal of Climate*, *28*(20), 8219-8246. Retrieved from https://journals.ametsoc.org/view/journals/clim/28/20/jcli-d-15-0148.1.xml doi: 10.1175/jcli-d-15-0148.1

Andrews, T., Forster, P. M., Boucher, O., Bellouin, N., & Jones, A. (2010). Precipitation, radiative forcing and global temperature change. *Geophysical Research Letters*, *37*(14). Retrieved 2020-09-04, from https://agupubs.onlinelibrary.wiley.com/doi/abs/10.1029/2010GL043991 (_eprint: https://agupubs.onlinelibrary.wiley.com/doi/pdf/10.1029/2010GL043991) doi: 10.1029/2010GL043991

Bollasina, M. A., Ming, Y., & Ramaswamy, V. (2011). Anthropogenic aerosols and the weakening of the south asian summer monsoon [Journal Article]. *Science*, *334*(6055), 502-505. Retrieved from https://www.science.org/doi/abs/10.1126/science.1204994 doi: doi:10.1126/science.1204994

Chemke, R., & Dagan, G. (2018). The effects of the spatial distribution of direct anthropogenic aerosols radiative forcing on atmospheric circulation [Journal Article]. *Journal of Climate*, *31*(17), 7129-7145. Retrieved from https://journals.ametsoc.org/view/journals/clim/31/17/jcli-d-17-0694.1.xml doi: 10.1175/jcli-d-17-0694.1

Dagan, G., & Stier, P. (2020). Constraint on precipitation response to climate change by combination of atmospheric energy and water budgets [Journal Article]. *npj Climate and Atmospheric Science*, *3*(1). doi: 10.1038/s41612-020-00137-8

Dagan, G., Stier, P., & Watson-Parris, D. (2019a). Analysis of the atmospheric water budget for elucidating the spatial scale of precipitation changes under climate change [Journal Article]. *Geophys Res Lett*, *46*(17-18), 10504-10511. Retrieved from https://www.ncbi.nlm.nih.gov/pubmed/31762521 doi: 10.1029/2019GL084173

Dagan, G., Stier, P., & Watson-Parris, D. (2019b). Contrasting response of precipitation to aerosol perturbation in the tropics and extratropics explained by energy budget considerations [Journal Article]. *Geophys Res Lett*, *46*(13), 7828-7837. Retrieved from https://www.ncbi.nlm.nih.gov/pubmed/31598021 doi: 10.1029/2019GL083479

Dagan, G., Stier, P., & Watson-Parris, D. (2021). An Energetic View on the Geographical Dependence of the Fast Aerosol Radiative Ef-

fects on Precipitation. *Journal of Geophysical Research: Atmospheres*, *126*(9), e2020JD033045. Retrieved 2021-05-28, from https://agupubs.onlinelibrary.wiley.com/doi/abs/10.1029/2020JD033045 (_eprint: https://agupubs.onlinelibrary.wiley.com/doi/pdf/10.1029/2020JD033045) doi: https://doi.org/10.1029/2020JD033045

DeAngelis, A. M., Qu, X., Zelinka, M. D., & Hall, A. (2015, December). An observational radiative constraint on hydrologic cycle intensification. *Nature*, *528*(7581), 249–253. Retrieved 2020-05-22, from https://www.nature.com/articles/nature15770 (Number: 7581 Publisher: Nature Publishing Group) doi: 10.1038/nature15770

Eyring, V., Bony, S., Meehl, G. A., Senior, C. A., Stevens, B., Stouffer, R. J., & Taylor, K. E. (2016, May). Overview of the Coupled Model Intercomparison Project Phase 6 (CMIP6) experimental design and organization. *Geoscientific Model Development*, *9*(5), 1937–1958. Retrieved 2019-11-15, from https://www.geosci-model-dev.net/9/1937/2016/ doi: 10.5194/gmd-9-1937-2016

Held, I. M., & Soden, B. J. (2006). Robust responses of the hydrological cycle to global warming [Journal Article]. *Journal of Climate*, *19*(21), 5686-5699. Retrieved from https://journals.ametsoc.org/view/journals/clim/19/21/jcli3990.1.xml doi: 10.1175/jcli3990.1

Laakso, A., Snyder, P. K., Liess, S., Partanen, A.-I., & Millet, D. B. (2020, May). Differing precipitation response between solar radiation management and carbon dioxide removal due to fast and slow components. *Earth System Dynamics*, *11*(2), 415–434. Retrieved 2021-12-22, from https://esd.copernicus.org/articles/11/415/2020/ (Publisher: Copernicus GmbH) doi: 10.5194/esd-11-415-2020

Lacis, A. A., & Hansen, J. (1974, January). A Parameterization for the Absorption of Solar Radiation in the Earth's Atmosphere. *Journal of the Atmospheric Sciences*, *31*(1), 118–133. Retrieved 2021-12-22, from https://journals.ametsoc.org/view/journals/atsc/31/1/1520-0469_1974_031_0118_apftao_2_0_co_2.xml (Publisher: American Meteorological Society Section: Journal of the Atmospheric Sciences) doi: 10.1175/1520-0469(1974)031⟨0118:APFTAO⟩2.0.CO;2

Lund, M. T., Myhre, G., & Samset, B. H. (2019, November). Anthropogenic aerosol forcing under the Shared Socioeconomic Pathways. *Atmospheric Chemistry and Physics*, *19*(22), 13827–13839. Retrieved 2020-05-22, from https://www.atmos-chem-phys.net/19/13827/2019/ (Publisher: Copernicus GmbH) doi: https://doi.org/10.5194/acp-19-13827-2019

Meinshausen, M., Nicholls, Z. R. J., Lewis, J., Gidden, M. J., Vogel, E., Freund, M., ... Wang, R. H. J. (2020). The shared socio-economic pathway (ssp) greenhouse gas concentrations and their extensions to 2500 [Journal Article]. *Geoscientific Model Development*, *13*(8), 3571-3605. doi: 10.5194/gmd-13-3571-2020

Myhre, G., Samset, B. H., Schulz, M., Balkanski, Y., Bauer, S., Berntsen, T. K., ... Zhou, C. (2013). Radiative forcing of the direct aerosol effect from aerocom phase ii simulations [Journal Article]. *Atmospheric Chemistry and Physics*, *13*(4), 1853-1877. doi: 10.5194/acp-13-1853-2013

Neill, B. C., Tebaldi, C., van Vuuren, D. P., Eyring, V., Friedlingstein, P., Hurtt, G., ... Sanderson, B. M. (2016). The scenario model intercomparison project (scenariomip) for cmip6 [Journal Article]. *Geoscientific Model Development*, *9*(9), 3461-3482. doi: 10.5194/gmd-9-3461-2016

Pendergrass, A. G. (2020). The global-mean precipitation response to co 2 -induced warming in cmip6 models [Journal Article]. *Geophysical Research Letters*, *47*(17). doi: 10.1029/2020gl089964

Pendergrass, A. G., & Hartmann, D. L. (2012). Global-mean pre-

cipitation and black carbon in AR4 simulations. *Geophysical Research Letters*, *39*(1). Retrieved 2020-05-22, from https://agupubs.onlinelibrary.wiley.com/doi/abs/10.1029/2011GL050067 (_eprint: https://agupubs.onlinelibrary.wiley.com/doi/pdf/10.1029/2011GL050067) doi: 10.1029/2011GL050067

Pendergrass, A. G., & Hartmann, D. L. (2014). The atmospheric energy constraint on global-mean precipitation change [Journal Article]. *Journal of Climate*, *27*(2), 757-768. doi: 10.1175/jcli-d-13-00163.1

Riahi, K., van Vuuren, D. P., Kriegler, E., Edmonds, J., O'Neill, B. C., Fujimori, S., ... Tavoni, M. (2017). The shared socioeconomic pathways and their energy, land use, and greenhouse gas emissions implications: An overview [Journal Article]. *Global Environmental Change*, *42*, 153-168. doi: 10.1016/j.gloenvcha.2016.05.009

Richardson, T. B., Forster, P. M., Andrews, T., Boucher, O., Faluvegi, G., Fläschner, D., ... Voulgarakis, A. (2018). Drivers of precipitation change: An energetic understanding [Journal Article]. *Journal of Climate*, *31*(23), 9641-9657. doi: 10.1175/jcli-d-17-0240.1

Samset, B. H., Myhre, G., Forster, P. M., Hodnebrog, , Andrews, T., Boucher, O., ... Voulgarakis, A. (2018, January). Weak hydrological sensitivity to temperature change over land, independent of climate forcing. *npj Climate and Atmospheric Science*, *1*(1), 1–8. Retrieved 2021-07-16, from https://www.nature.com/articles/s41612-017-0005-5 (Bandiera_abtest: a Cc_license_type: cc_by Cg_type: Nature Research Journals Number: 1 Primary_atype: Research Publisher: Nature Publishing Group Subject_term: Climate and Earth system modelling;Projection and prediction Subject_term_id: climate-and-earth-system-modelling;projection-and-prediction) doi: 10.1038/s41612-017-0005-5

Samset, B. H., Myhre, G., Forster, P. M., Hodnebrog, , Andrews, T., Faluvegi, G., ... Voulgarakis, A. (2016). Fast and slow precipitation responses to individual climate forcers: A pdrmip multimodel study [Journal Article]. *Geophysical Research Letters*, *43*(6), 2782-2791. doi: 10.1002/2016gl068064

Turnock, S. T., Allen, R. J., Andrews, M., Bauer, S. E., Deushi, M., Emmons, L., ... Zhang, J. (2020, November). Historical and future changes in air pollutants from CMIP6 models. *Atmospheric Chemistry and Physics*, *20*(23), 14547–14579. Retrieved 2021-11-16, from https://acp.copernicus.org/articles/20/14547/2020/ (Publisher: Copernicus GmbH) doi: 10.5194/acp-20-14547-2020

Wang, C. (2015). Anthropogenic aerosols and the distribution of past large-scale precipitation change [Journal Article]. *Geophys Res Lett*, *42*(24), 10876-10884. Retrieved from https://www.ncbi.nlm.nih.gov/pubmed/27134319 doi: 10.1002/2015GL066416

Supporting Information for *Absorbing aerosol choices influence precipitation changes across future scenarios*

Isabel L. McCoy[1,2], Mika Vogt[3], and Robert Wood[3]

[1]Rosenstiel School of Marine and Atmospheric Science, University of Miami, Miami, FL, 33149-1031, USA

[2]Cooperative Programs for the Advancement of Earth System Science, University Corporation for Atmospheric Research, Boulder, CO, 80307-3000, USA

[3]Department of Atmospheric Sciences, University of Washington, Seattle, WA, 98195-1640, USA

Contents of this file

1. Tables S1 to S5
2. Figures S1 to S6

0094-8276/22/$5.00

Table S1. Individual CMIP6 Models used in ScenarioMIP Ensemble

Model	Member
CanESM5	r1i1p1f1
CESM2-WACCM	r1i1p1f1
CMCC-CM2-SR5	r1i1p1f1
CMCC-ESM2	r1i1p1f1
CNRM-CM6-1	r1i1p1f2
CNRM-CM6-1-HR	r1i1p1f2
CNRM-ESM2-1	r1i1p1f2
GFDL-ESM4	r1i1p1f1
INM-CM4-8	r1i1p1f1
INM-CM5-0	r1i1p1f1
IPSL-CM6A-LR	r1i1p1f1
MIROC6	r1i1p1f1
MIROC-ES2L	r1i1p1f2
MPI-ESM1-2-HR	r1i1p1f1
MPI-ESM1-2-LR	r1i1p1f1
MRI-ESM2-0	r1i1p1f1
NorESM2-LM	r1i1p1f1
UKESM1-0-LL	r1i1p1f2

Table S2. ScenarioMIP Global Ensemble Mean, SE Changes and Quantities

Variable	Units	SSP1-2.6	SSP2-4.5	SSP3-7.0	SSP5-8.5
ΔT	K	0.78±0.04	1.83±0.09	3.00±0.15	3.92±0.20
ΔWVP	kgm^{-2}	1.30±0.07	3.29±0.17	5.74±0.29	7.75±0.39
$\Delta AAOD$	$\cdot 10^{-3}$	-1.67±0.08	-1.76±0.09	0.15±0.02	-1.19±0.05
ΔCO_2*	ppm	37.8	187.9	416.7	660.0
ΔCH_4	ppb	-795±7	-203±12	1386±22	576±17
ΔSW	Wm^{-2}	-0.03±0.02	1.18±0.06	3.51±0.17	3.83±0.20
ΔLW	Wm^{-2}	-2.00±0.11	-3.98±0.20	-6.24±0.31	-8.08±0.41
ΔSH	Wm^{-2}	0.095±0.006	-0.34±0.02	-0.98±0.05	-0.97±0.05
ΔLH	Wm^{-2}	2.01±0.10	3.27±0.17	3.86±0.19	5.41±0.27
η	$Wm^{-2}K^{-1}$	2.21±0.22	2.06±0.26	1.86±0.25	1.84±0.28
$\overline{\eta_{SSP}}$	1.99 ± 0.25	-	-	-	-
η_a	$Wm^{-2}K^{-1}$	2.54±0.16	1.76±0.07	1.30±0.07	1.39±0.07
ΔP	Wm^{-2}	2.00±0.10	3.23±0.17	3.90±0.20	5.44±0.27
ΔP_{fast}	Wm^{-2}	0.43±0.27	-0.42±0.48	-2.07±0.80	-2.35±1.04
$\Delta P_{fastCO2}$	Wm^{-2}	-0.28±0.02	-1.19±0.10	-2.21±0.19	-3.02±0.26
$\Delta P_{fastCH4}$	Wm^{-2}	0.25±0.05	0.05±0.01	-0.25±0.05	-0.12±0.02
$\Delta P_{fastAAOD}$	Wm^{-2}	0.46±0.27	0.72±0.49	0.39±0.83	0.79±1.07
$\Delta P_{fastAAOD}P20$	Wm^{-2}	0.33±0.26	0.41±0.50	-0.12±0.84	0.13±1.08
ΔP_{AAOD}	Wm^{-2}	0.62±0.25	0.65±0.27	-0.05±0.34	0.45±0.28
ΔSW_{AAOD}	Wm^{-2}	-0.87±0.04	-0.91±0.05	0.08±0.01	-0.62±0.03

* CO_2 is prescribed in ScenarioMIP simulations thus no SE is reported.

Table S3. Mean, SE for Global Energy Budget Changes from Figure 2

Variable	Units	SSP2-4.5	SSP3-7.0
ΔSW	$Wm^{-2}K^{-1}$	0.64±0.09	1.2±0.2
ΔSW_{AAOD}	$Wm^{-2}K^{-1}$	-0.50±0.07	0.026±0.007
ΔSW_{WVP}	$Wm^{-2}K^{-1}$	1.1±0.2	1.1±0.2
ΔLW	$Wm^{-2}K^{-1}$	-2.2±0.3	-2.1±0.3
ΔSH	$Wm^{-2}K^{-1}$	-0.19±0.03	-0.33±0.05
$\Delta LH = L_v \Delta P$	$Wm^{-2}K^{-1}$	1.8±0.3	1.3±0.2

Table S4. ScenarioMIP Regional Ensemble Mean, SE for $\Delta AAOD$

Region	Units	SSP1-2.6	SSP2-4.5	SSP3-7.0	SSP5-8.5
Global	$\cdot 10^{-3}$	-1.67±0.08	-1.76±0.09	0.15±0.02	-1.19±0.05
Southeast Asia	$\cdot 10^{-3}$	-8.28±0.40	-9.12±0.49	-1.74±0.18	-8.85±0.42
Equatorial Africa	$\cdot 10^{-3}$	-2.95±0.13	-4.98±0.29	2.97±0.15	1.11±0.25

Table S5. Mean, SE for Regional Budget Changes from Figures 3 and 4

Variable	Units	SSP2-4.5	SSP3-7.0
Southeast Asia (0-45°N, 60-130°E)			
$L_v\Delta P$	$Wm^{-2}K^{-1}$	4.0±0.6	2.6±0.4
$L_v\Delta P_{thermo}$	$Wm^{-2}K^{-1}$	4.8±0.8	3.6±0.5
$L_v\Delta P_{circ}$	$Wm^{-2}K^{-1}$	-0.8±0.8	-1.0±0.5
ΔSW	$Wm^{-2}K^{-1}$	-0.7±0.1	1.1±0.2
ΔSW_{AAOD}	$Wm^{-2}K^{-1}$	-2.6±0.4	-0.30±0.07
ΔSW_{WVP}	$Wm^{-2}K^{-1}$	1.5±0.4	1.5±0.4
ΔLW	$Wm^{-2}K^{-1}$	-2.4±0.3	-2.6±0.4
ΔSH	$Wm^{-2}K^{-1}$	0.58±0.09	-0.11±0.02
$\Delta div(s)$	$Wm^{-2}K^{-1}$	1.5±0.6	1.0±0.4
$\Delta div(q_v)$	$Wm^{-2}K^{-1}$	-1.1±0.6	-0.9±0.4
$\Delta div(q_v)_{thermo}$	$Wm^{-2}K^{-1}$	-1.9±1.0	-1.9±0.8
$\Delta div(q_v)_{circ}$	$Wm^{-2}K^{-1}$	0.8±1.1	1.0±0.9
ΔLH	$Wm^{-2}K^{-1}$	2.8±0.4	1.7±0.2
Equatorial Africa (15°S-15°N, 30°W-30°E)			
$L_v\Delta P$	$Wm^{-2}K^{-1}$	1.6±0.3	1.3±0.3
$L_v\Delta P_{thermo}$	$Wm^{-2}K^{-1}$	2.1±0.5	1.0±0.3
$L_v\Delta P_{circ}$	$Wm^{-2}K^{-1}$	-0.6±0.6	0.3±0.4
ΔSW	$Wm^{-2}K^{-1}$	0.10±0.07	1.7±0.2
ΔSW_{AAOD}	$Wm^{-2}K^{-1}$	-1.4±0.2	0.51±0.07
ΔSW_{WVP}	$Wm^{-2}K^{-1}$	1.7±0.5	1.6±0.5
ΔLW	$Wm^{-2}K^{-1}$	-2.7±0.4	-2.5±0.4
ΔSH	$Wm^{-2}K^{-1}$	0.47±0.08	-0.14±0.03
$\Delta div(s)$	$Wm^{-2}K^{-1}$	-0.6±0.4	0.3±0.4
$\Delta div(q_v)$	$Wm^{-2}K^{-1}$	1.2±0.4	0.3±0.3
$\Delta div(q_v)_{thermo}$	$Wm^{-2}K^{-1}$	0.6±0.2	0.6±0.5
$\Delta div(q_v)_{circ}$	$Wm^{-2}K^{-1}$	0.6±0.5	-0.3±0.6
ΔLH	$Wm^{-2}K^{-1}$	2.7±0.4	1.6±0.2

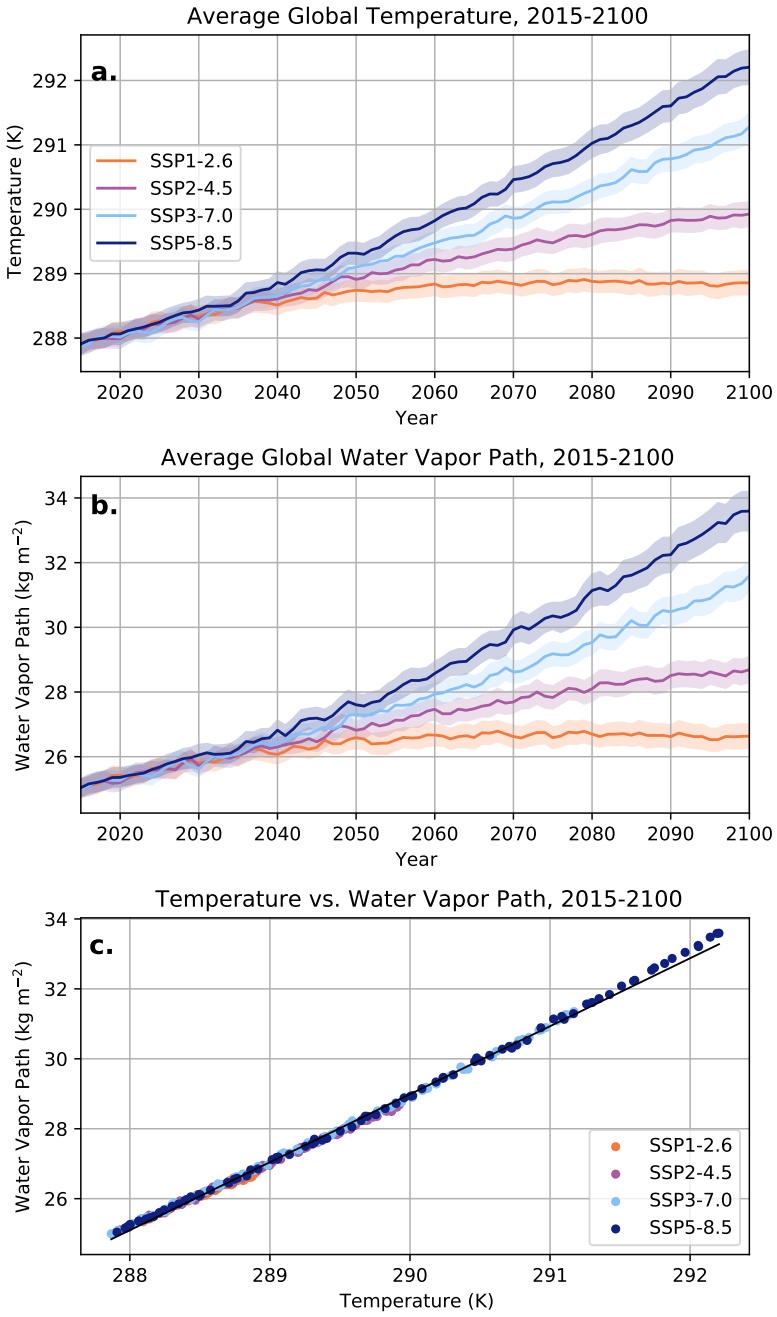

Figure S1. Global multi-model ensemble mean (line) and corresponding standard error (shading) by scenario across period of interest (2015-2100) for (a) temperature and (b) water vapor path. (c) The global multi-model ensemble mean temperature is correlated with water vapor path at R^2= 0.997 at 95% confidence and has a slope of m= 1.94 kg m^{-2} K^{-1}.

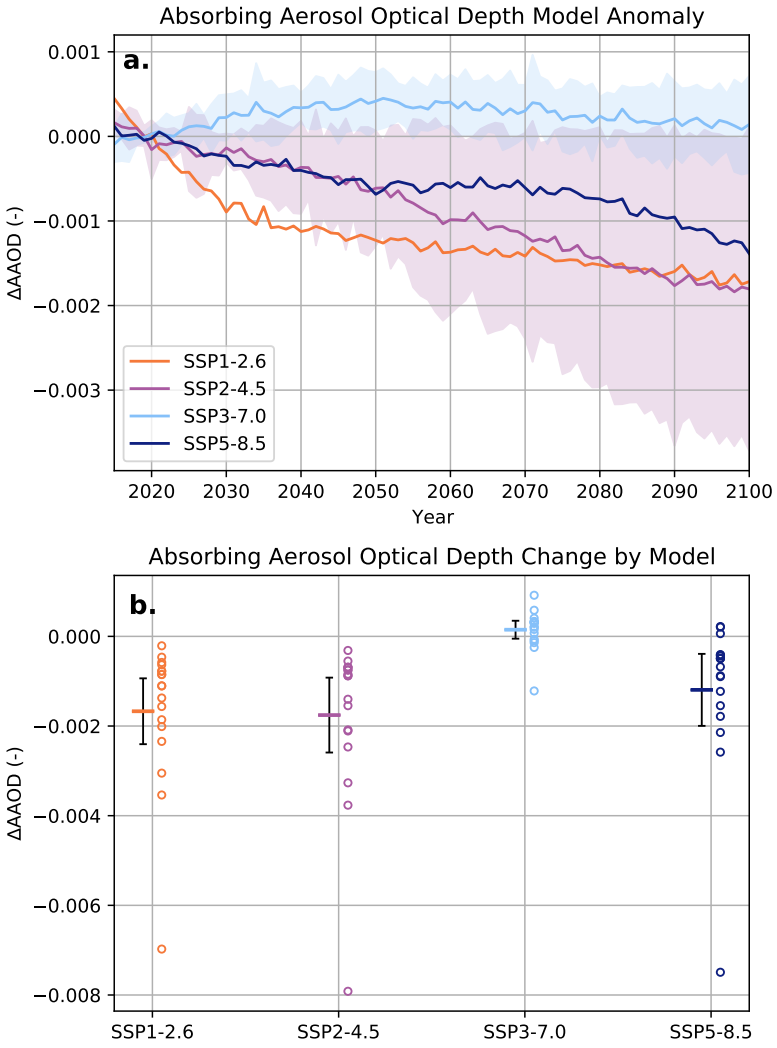

Figure S2. (a) SSP multi-model mean of trends in the anomaly of $AAOD$ from the 2015-2025 period. Standard deviations are included for SSP2-4.5 and SSP3-7.0. (b) Global mean $\Delta AAOD$ for individual CMIP6 models (circles) with mean (horizontal bar) and 2SE (error bars) for all scenarios.

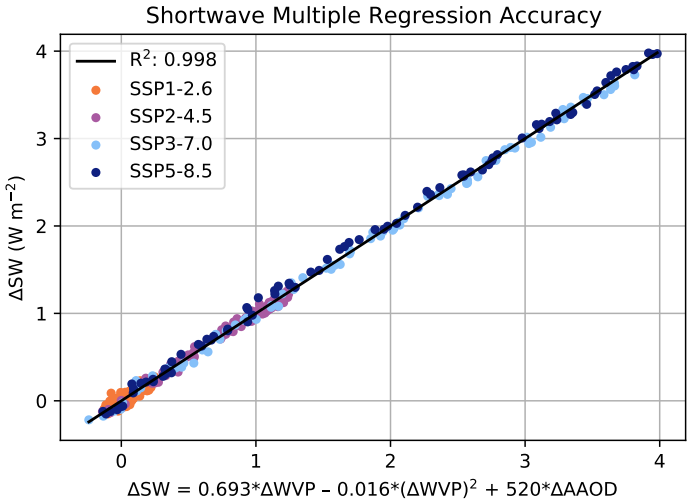

Figure S3. CMIP6 SSP change in SW vs. predicted change in SW based on changes in WVP and AAOD from Eq. 2. Each scatter point represents a year from 2015-2100.

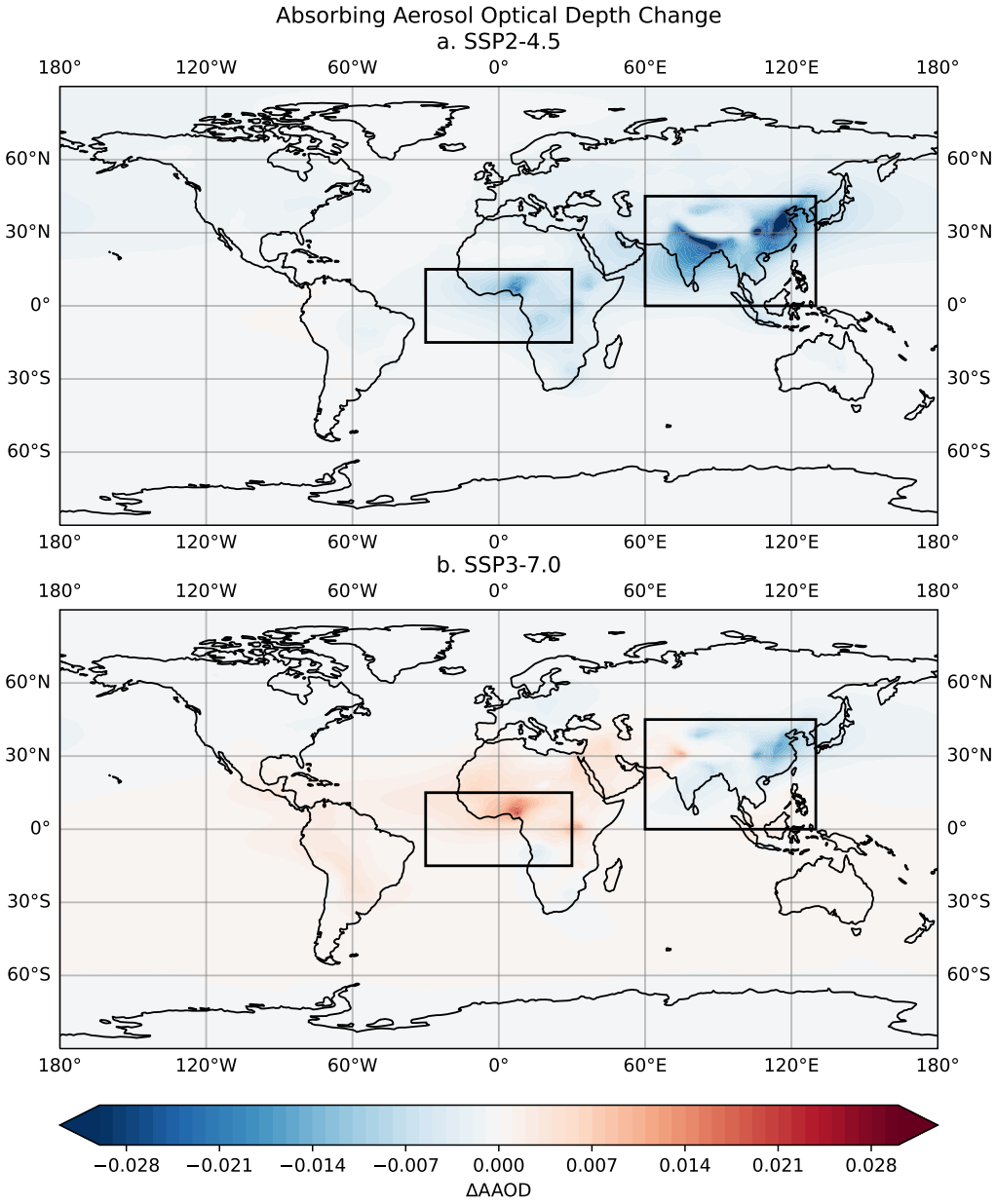

Figure S4. Global changes in AAOD between 2015-2025 and 2090-2100 for two CMIP6 SSP simulations with contrasting aerosol choices: (a) SSP2-4.5 (*Middle of the road*) and (b) SSP3-7.0 (*Regional Rivalry*). Two regions of interest are highlighted: Southeast Asia (0-45°N, 60-130°E) which experiences decreases in AAOD in both (a, b) and Equatorial Africa (15°S-15°N, 30°W-30°E) which experiences decreases in AAOD in (a) but increases in (b). See Table S4 for values.

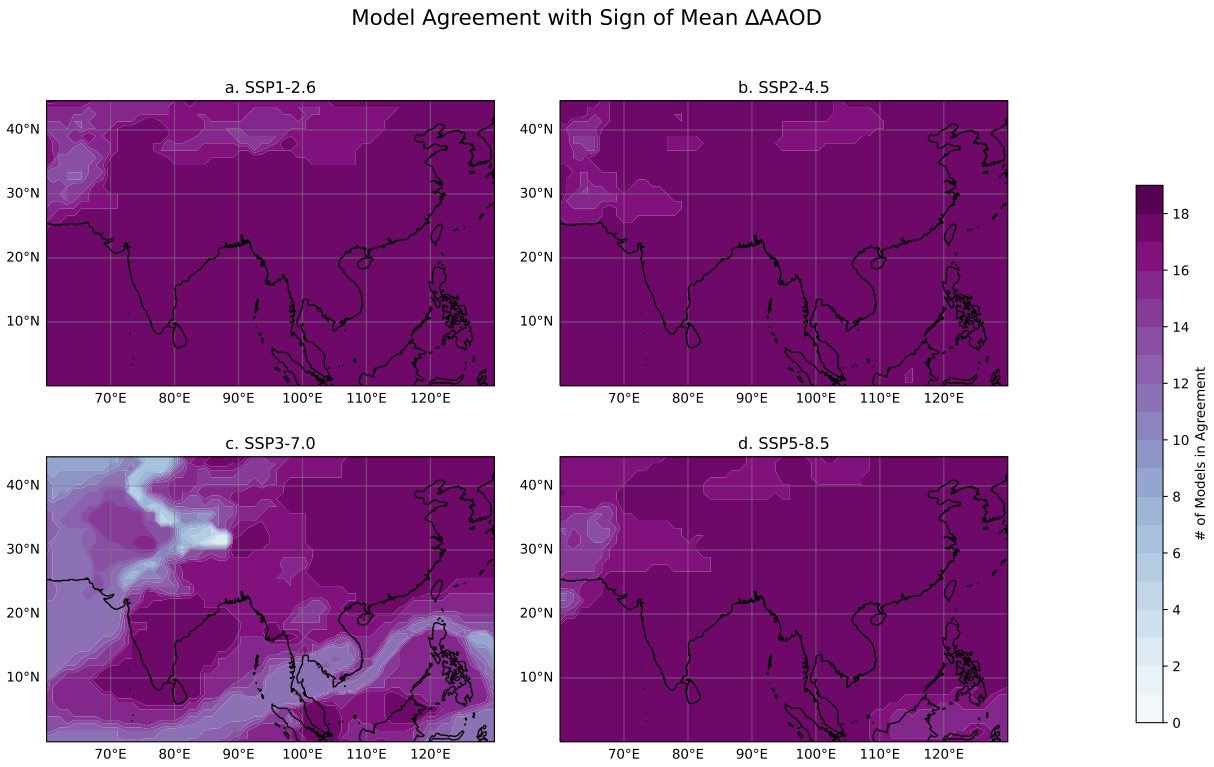

Figure S5. Number of CMIP6 models that agree in the sign of the regional $\Delta AAOD$ in Southeast Asia (0-45°N, 60-130°E) between 2015-2025 and 2090-2100 for four ScenarioMIP simulations: (a) SSP1-2.6, (b) SSP2-4.5, (c) SSP3-7.0, and (d) SSP5-8.5.

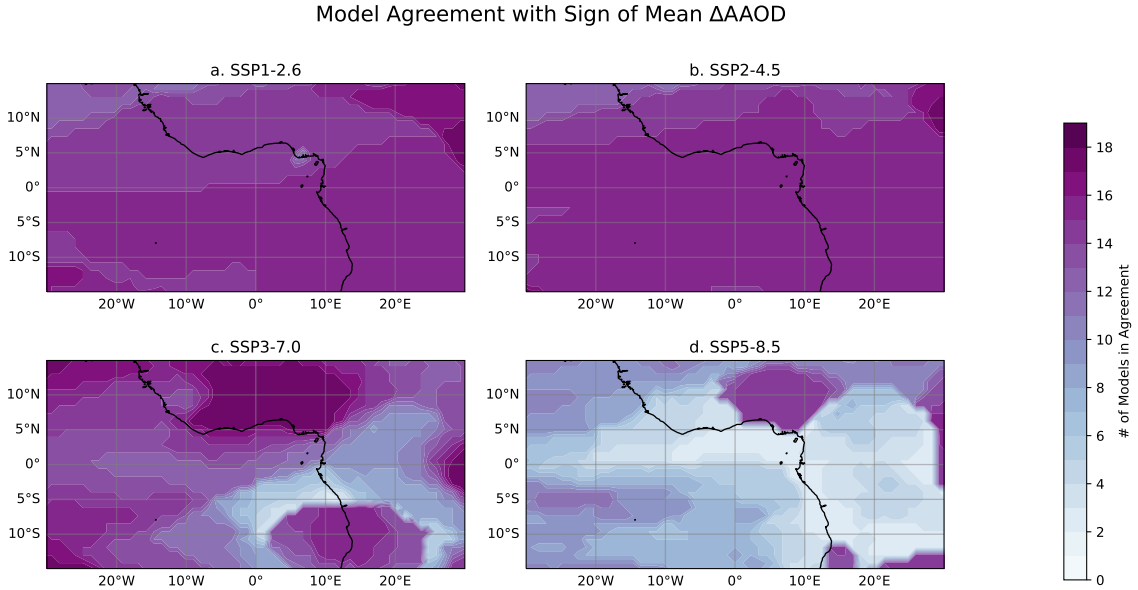

Figure S6. Number of CMIP6 models that agree in the sign of the regional $\Delta AAOD$ in Equatorial Africa (15°S-15°N, 30°W-30°E) between 2015-2025 and 2090-2100 for four ScenarioMIP simulations: (a) SSP1-2.6, (b) SSP2-4.5, (c) SSP3-7.0, and (d) SSP5-8.5.